

# Bidirectional Temporal Dynamics Modeling for EEG-based Driving Fatigue Recognition

Yip Tin Po\*, Jianming Wang\*, Yutao Miao, Jiayan Zhang, Yunxu Zhao,  
Xiaomin Ouyang, Zhihong Li, Nevin L. Zhang

**Abstract**—Driving fatigue is a major contributor to traffic accidents and poses a serious threat to road safety. Electroencephalography (EEG) provides a direct measurement of neural activity, yet EEG-based fatigue recognition is hindered by strong non-stationarity and asymmetric neural dynamics. To address these challenges, we propose DeltaGateNet, a novel framework that explicitly captures Bidirectional temporal dynamics for EEG-based driving fatigue recognition. Our key idea is to introduce a Bidirectional Delta module that decomposes first-order temporal differences into positive and negative components, enabling explicit modeling of asymmetric neural activation and suppression patterns. Furthermore, we design a Gated Temporal Convolution module to capture long-term temporal dependencies for each EEG channel using depthwise temporal convolutions and residual learning, preserving channel-wise specificity while enhancing temporal representation robustness. Extensive experiments conducted under both intra-subject and inter-subject evaluation settings on the public SEED-VIG and SADT driving fatigue datasets demonstrate that DeltaGateNet consistently outperforms existing methods. On SEED-VIG, DeltaGateNet achieves an intra-subject accuracy of 81.89% and an inter-subject accuracy of 55.55%. On the balanced SADT 2022 dataset, it attains intra-subject and inter-subject accuracies of 96.81% and 83.21%, respectively, while on the unbalanced SADT 2952 dataset, it achieves 96.84% intra-subject and 84.49% inter-subject accuracy. These results indicate that explicitly modeling Bidirectional temporal dynamics yields robust and generalizable performance under varying subject and class-distribution conditions.

**Index Terms**—Driving fatigue recognition, Electroencephalography (EEG), DeltaGateNet, Bidirectional Delta, Gated Temporal Convolution

## I. INTRODUCTION

**D**RIVING fatigue is widely recognized as one of the leading contributors to traffic accidents worldwide, particularly in long-duration and monotonous driving scenarios [1]. Recent large-scale studies have shown that fatigue-related impairment can increase the risk of severe traffic accidents by several fold, posing a significant threat to public safety and transportation systems [2]. Unlike alcohol or distraction, fatigue is a latent and gradually accumulated cognitive state, which makes it difficult to be reliably detected through self-report or post-event analysis. Therefore, developing an objective, real-time, and reliable driving fatigue recognition system remains a critical yet unresolved challenge.

Existing driving fatigue detection approaches can be broadly categorized into non-physiological and physiological methods [3]. Non-physiological techniques, such as behavioral analysis, vehicle dynamics monitoring, and vision-based methods, are

often sensitive to environmental conditions and provide limited interpretability of the driver's internal cognitive state [4], [5]. In contrast, physiological approaches—particularly those based on electroencephalography (EEG)—offer a more direct and objective measurement of neural activity associated with vigilance and fatigue. However, many EEG-based methods still rely on handcrafted spectral features or static representations, which inadequately characterize the temporal evolution of fatigue-related neural processes [6], [7]. Although recent deep learning models have demonstrated improved representation learning capability, most existing architectures primarily focus on amplitude-based features or generic temporal modeling, while largely overlooking the Bidirectional nature of neural dynamics and the inherent channel-wise independence of EEG recordings [8], [9].

The previously mentioned constraints arise mainly from the complex temporal properties of the EEG data, which present considerable obstacles to the reliable identification of driving fatigue. Initially, EEG data exhibit significant non-stationarity, with fatigue presenting as slow and irregular temporal variations instead of sudden state transitions [10]. Secondly, fatigue-associated brain mechanisms demonstrate significant bidirectional asymmetry, since reductions in arousal and compensatory neural activation do not adhere to symmetrical temporal patterns [11], [12]. Third, practical driving applications often depend on a restricted number of EEG channels, which limits spatial information and requires a stronger focus on robust channel-specific temporal modeling [13], [14]. These constraints collectively constrain the efficiency and generalizability of current EEG-based fatigue identification techniques, especially in real-world and cross-subject application scenarios.

Drawing from previous studies on non-stationary EEG modeling, asymmetric brain processing, and temporal convolutional networks, the key insight is that driving fatigue is more accurately defined by the temporal evolution of neural activity than by its absolute amplitude [10]. Bidirectional temporal variations in EEG signals offer essential insights into the decline of focus and brain inhibition mechanisms. Based on these insights, we propose a new framework called DeltaGateNet that directly models bidirectional temporal dynamics using a Bidirectional Delta module and captures long-term dependencies using a Gated Temporal Convolution module. The Bidirectional Delta module splits time variations into positive and negative components, allowing the network to differentiate between asymmetric neuronal activation and suppression patterns. The Gated Temporal Convolution module tracks temporal dynamics for each EEG channel through

\*These authors contributed equally to this work.

depthwise temporal convolutions and residual learning, maintaining spatial distinctiveness while accumulating long-range temporal information.

Comprehensive studies performed on two public driving fatigue datasets, SEED-VIG and SADT, in both intra-subject and inter-subject evaluation settings demonstrate the effectiveness and robustness of the proposed DeltaGateNet. DeltaGateNet achieves an intra-subject accuracy of 81.89% and an inter-subject accuracy of 55.55% on the SEED-VIG dataset. In the balanced SADT 2022 dataset, the proposed method obtains intra-subject and inter-subject accuracies of 96.81% and 83.21%, respectively. Significantly, similar performance is found on the unbalanced SADT 2952 dataset, with DeltaGateNet reaching 96.84% intra-subject accuracy and 84.49% inter-subject accuracy. The results demonstrate that explicitly modeling bidirectional temporal dynamics and channel-wise temporal dependencies facilitates robust and generalizable detection of driving fatigue based on EEG, even under diverse subject distributions and conditions of class imbalance.

**The main contributions of this work are summarized as follows:**

- We propose DeltaGateNet, a novel EEG-based driving fatigue recognition framework that explicitly models Bidirectional temporal dynamics through a Bidirectional Delta module and captures long-term fatigue-related dependencies using a Gated Temporal Convolution module, enabling effective channel-wise temporal representation under limited EEG channel configurations.
- We conducted extensive experiments on two public datasets on driving fatigue, SEED-VIG and SADT, under both intra-subject and inter-subject evaluation settings. The proposed method consistently outperforms existing approaches and demonstrates robust performance across balanced and unbalanced class distributions.
- To facilitate reproducibility and future research, DeltaGateNet implementation will be released as an open-source project at <https://jianmingwang1998.github.io/DeltaGateNet/>. The code will be released after acceptance.

## II. RELATED WORKS

Driving fatigue recognition based on EEG is inherently a temporal modeling problem, as fatigue reflects a gradual, accumulative, and often asymmetric degradation of cognitive states over time. From a modeling perspective, existing end-to-end EEG-based driving fatigue recognition methods can be systematically categorized according to how temporal dynamics are represented and constrained. From this perspective, previous research can be categorized into four paradigms: (1) implicit temporal aggregation, (2) multi-scale symmetric temporal modeling, (3) global temporal dependency modeling, and (4) lightweight and physiologically limited temporal modeling.

### A. Implicit Temporal Aggregation

Early deep learning methodologies for EEG-based driving fatigue detection mostly utilize convolutional neural networks

that implicitly capture temporal information by using fixed-size temporal kernels and pooling processes. In these methods, temporal dynamics are not explicitly modeled but are instead embedded as latent features during network optimization. Representative studies employ covariance-based CNNs to capture inter-channel relationships from EEG epochs [15], or compact convolutional architectures to extract fatigue-related patterns from single-channel or low-density EEG recordings [16]. These designs reduce reliance on handcrafted elements and exhibit commendable performance, especially in intra-subject evaluation contexts.

However, implicit temporal aggregation assumes that fatigue-related EEG features may be sufficiently captured within constrained temporal receptive fields. This assumption is limiting for driving fatigue, which develops continually and nonlinearly throughout extended driving durations. Thus, models that depend exclusively on implicit temporal encoding frequently demonstrate constrained sensitivity to subtle vigilance transitions and reduced robustness in cross-subject evaluations.

### B. Multi-Scale Symmetric Temporal Modeling

To mitigate the constraints of fixed temporal receptive fields, further research introduces explicit multi-scale temporal modeling methodologies. Fully convolutional networks and Inception-style architectures utilize parallel temporal convolutions with diverse kernel sizes to capture EEG fluctuations at multiple temporal resolutions [17], [18]. InceptionTime and its associated versions illustrate this paradigm by concurrently simulating short-term fluctuations and long-term temporal patterns. Residual temporal convolutional networks improve training stability and feature propagation through skip connections, exhibiting robust performance in various time-series classification tasks [17], [19].

While multi-scale temporal modeling improves the representation of heterogeneous temporal patterns, these methods predominantly treat temporal variations in a symmetric manner, focusing on amplitude-based feature extraction. As a result, they fail to explicitly capture the Bidirectional characteristics of temporal evolution, such as progressive enhancement or attenuation of neural activity, which are closely associated with fatigue accumulation and vigilance decline.

### C. Global Temporal Dependency Modeling

More recently, attention-based architectures, including Transformer and Vision Transformer variants, have been introduced to EEG analysis to explicitly model long-range temporal dependencies. By leveraging self-attention mechanisms, these models can capture interactions across distant time points and channels. Hybrid CNN-Transformer frameworks combine local convolutional feature extraction with global attention modeling [20], while ViT-based approaches reinterpret EEG signals as sequences of patches or time-frequency representations [21].

Despite their expressive power, global dependency models generally require large-scale datasets and incur substantial

computational overhead. Moreover, most existing attention-based approaches aim to learn generic temporal relationships without explicitly encoding the Bidirectionality of temporal changes or preserving channel-wise temporal independence. These limitations reduce their practicality for EEG-based driving fatigue recognition, particularly in real-world scenarios involving limited-channel wearable devices and constrained data availability.

#### D. Lightweight and Physiologically Constrained Temporal Modeling

In parallel, a line of research focuses on lightweight and physiologically motivated EEG networks that balance performance, interpretability, and computational efficiency. EEGNet is a representative example that decouples spatial and temporal feature learning through depthwise and separable convolutions, achieving competitive performance with significantly reduced model complexity [22]. Subsequent studies adapt such compact architectures to fatigue-related tasks by adjusting temporal kernel sizes, normalization strategies, and pooling operations [23].

Although these models are well suited for real-time and wearable applications, their temporal modeling capacity remains largely implicit and constrained by predefined architectural assumptions. In particular, they do not explicitly model asymmetric or Bidirectional temporal dynamics inherent in prolonged driving fatigue, limiting their ability to robustly characterize non-stationary vigilance degradation.

### III. METHODS

In this section, we propose an outstanding machine learning model that excels in driving fatigue detection on raw, unprocessed EEG signals. The overview of our model, Delta-GateNet, is shown in Fig. 1. In particular, the model consists of three simple but effective modules. Firstly, the Bidirectional Delta consists of no learnable parameters but is able to assist simple models to learn deeper representations of the EEG signal, which will be verified in Section V: Experimental Results. Secondly, the signals are passed to a Gated Temporal Convolution module, where EEG signals are further extracted and refined, turning into temporal encoded vectors of dimension  $H$ . Finally, the EEG signals are passed into a multilayer perceptron for processing and classification, producing three fatigue prediction heads corresponding to the three classes.

#### A. Bidirectional Delta Representations

In this module, we aim to extract the time derivative for each EEG input channel. For each EEG input channel, the algorithm computes  $\Delta x(t)$  that is denoted by the equation below:

$$\Delta x(t) = x(t) - x(t - 1) \quad \forall t \in \{1, 2, \dots, T - 1\}$$

This approximates the time differential of EEG signals, which measures the discrete difference. This highlights rapid changes like a high-pass filter, removing slow drifts and offsets that are prevalent in unprocessed and unfiltered EEG signals.

Then, the time derivatives are passed through the rectified linear unit that effectively separates positive differentials from negative differentials consisting of two tensors of shape  $x \in \mathbb{R}^{B \times C \times T}$  where  $B$  denotes the batch size,  $C$  denotes the number of EEG input channels and  $T$  denotes the number of timesteps. The rectified linear unit can be described by the equation:

$$\text{ReLU}(x) = \max(0, x)$$

The two tensors are then concatenated along the input channel dimension to form a single tensor of shape  $x \in \mathbb{R}^{B \times 2 \cdot C \times T}$ . Following the successful application of derivative features in audio signal processing for capturing temporal dynamics [24], this approach is adapted for EEG analysis. By explicitly providing the network with separated positive and negative first-order differentials, the model is endowed with direct access to the Bidirectional trends of the neural signal. Studies of brain responses to speech have found that including a half-wave rectified derivative of the speech envelope significantly boosts prediction accuracy [25]. This demonstrates that explicitly encoding the direction of change helps downstream modeling. These derivative features encode the rapid fluctuations and their polarity, allowing the network to learn distinct and complementary patterns for rising and falling waves independently. This results in stronger latent representations that are more invariant to inter-subject variance in EEG dynamics, as the model focuses on fundamental temporal shapes rather than absolute amplitudes.

#### B. Gated Temporal Convolution

Gating mechanisms in convolutional sequence models have strong theoretical and empirical support. The idea is to let a convolutional layer modulate its output through learned gates, which can control information flow. It has been proven that GLU-based CNNs converge faster and achieve lower perplexity than ReLU or tanh networks [26]. Similarly, WaveNet [27] and Graph-WaveNet [28] use gated dilated convolutions to capture long-range dependencies, which improves performance on audio and traffic forecasting. This inspired us to create a module that leverages the selective filtering properties offered by the GELU activation, hypothesizing that its intrinsic stochastic gating behavior, which smoothly retains or suppresses information based on magnitude, could be particularly effective for distilling meaningful neural oscillations from noisy, non-stationary EEG inputs.

Following the Bidirectional Delta module, a gated temporal convolution operates as the primary feature extraction block. Firstly, the tensor of size  $x \in \mathbb{R}^{B \times 2 \cdot C \times T}$  passed from the Bidirectional delta module undergoes a projection by a depthwise convolution of kernel size 1. This projects the signals to a new feature space where  $x \in \mathbb{R}^{B \times 2 \cdot C \cdot D \times T}$ , and  $D$  denotes the number of hidden dimensions. As a result, deeper feature representations are learned for each individual channel.

Next, the model stacks two residual layer blocks that enable stabilized training and allow the model refine features without losing the original input. Each residual block performs a 1D convolution of kernel size 7 and groups  $2 \cdot C \cdot D$  to extract the features of each channel depth. Since the kernel size is 1 x 7,

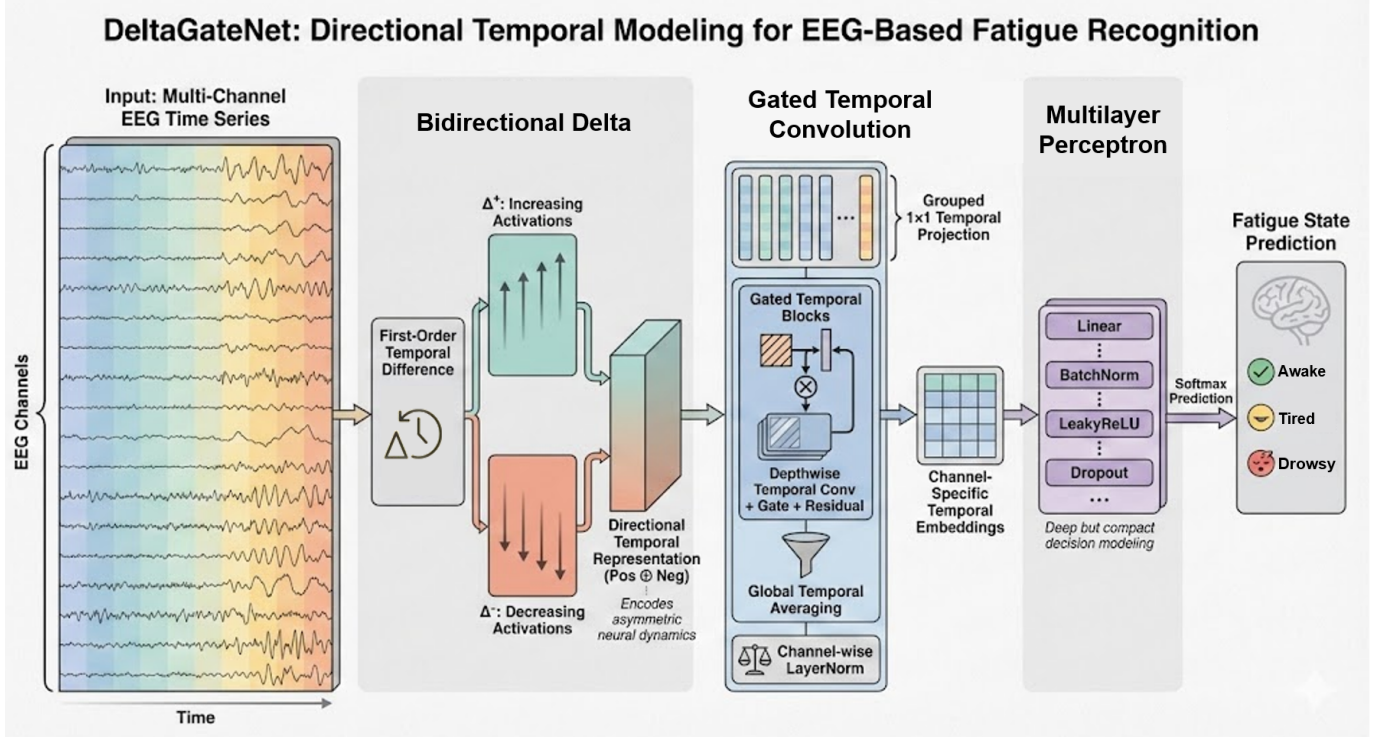


Fig. 1. Overview of the proposed DeltaGateNet. DeltaGateNet is a simple structure that contains three main components. Stage one is the Bidirectional Delta module that computes the differential across timesteps. Stage two is a gated temporal convolution block that encodes temporal features and selects activation using a soft gating mechanism. In stage three, the encoded temporal feature maps are fed into the multilayer perceptron that produces three probabilities representing the predicted classes. Note that under most experimental settings and datasets, fatigue levels increase concurrently with the time progresses, as subjects are more likely to grow tired towards the end of the experiment.

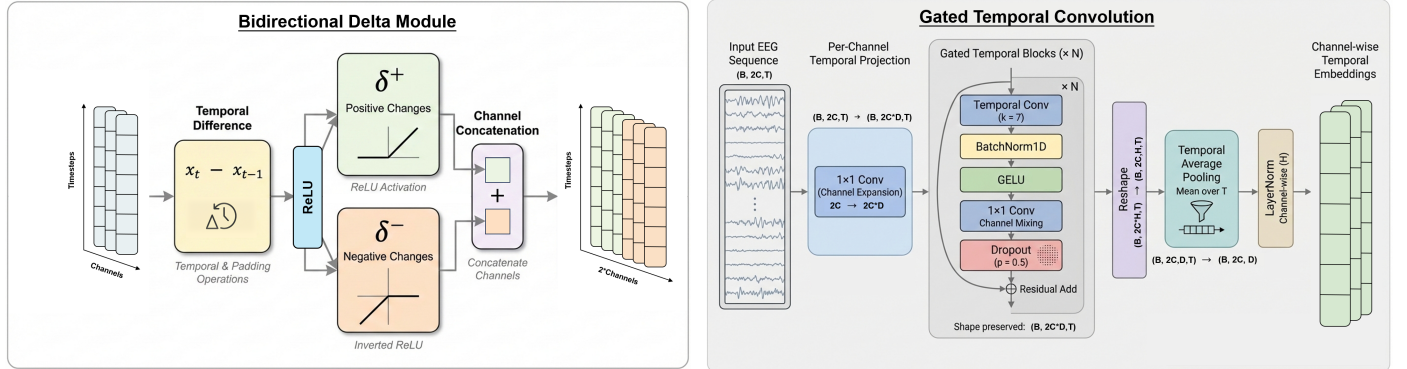


Fig. 2. The Bidirectional Delta module computes a first-order temporal difference that approximates the differential of EEG data as fatigue is encoded in changes over time. The module leverages the ReLU activation function to separate the changes into positive and negative differentials to contain richer temporal information for further processing.

the kernel extracts local temporal patterns in each channel's time series. Then, it is followed by a BatchNorm operation that aims to prevent internal covariate shift of features. A GELU gate is then employed to select features that are most relevant to be activated. The GELU activation is denoted as:

$$\text{GELU}(x) = x \cdot \Phi(x)$$

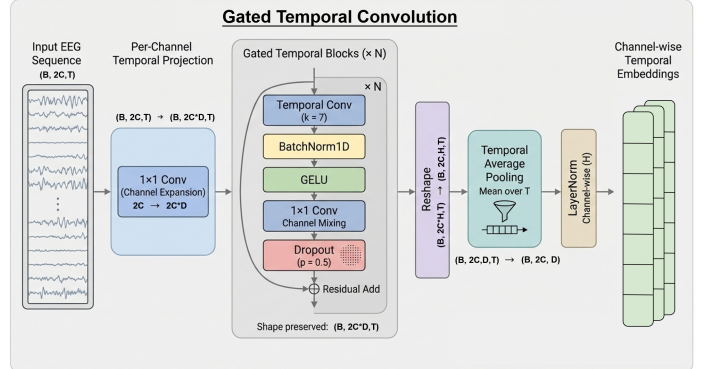


Fig. 3. The Gated Temporal Convolution projects the differentials to a higher-dimensional latent space to extract deeper information and then performs a local temporal convolution that captures short-term EEG signals. A GELU activation and 1x1 depthwise convolution block are utilized to select significant features to pass through. Residual blocks are used to select which features of signals to amplify or diminish.

or more commonly approximated as:

$$\text{GELU}(x) \approx 0.5x \left( 1 + \tanh \left( \sqrt{\frac{2}{\pi}} (x + 0.044715x^3) \right) \right)$$

The GELU activation function was employed because the Gaussian Error Linear Unit often outperforms conventional activations like ReLU and ELU. It has been reported that GELU has consistent gains over ReLU/ELU across vision, NLP, and speech tasks. These improvements are attributed

to GELU's smooth nonlinearity and nonzero gradients for negative inputs, which allow more nuanced gating of signals [29]. Afterwards, it is followed by a 1x1 convolution that mixes across feature channels. A dropout layer is then placed to prevent overfitting.

A residual layer assists in amplifying relevant signals or diminishing noisy signals [30]. Residual is defined as:

$$x \leftarrow x + f(x)$$

where  $x$  is the original input and  $f(x)$  is the processed input. The residual block amplifies certain temporal or channel wise patterns when  $f(x)$  is aligned with  $x$ , as  $f(x) \approx x$ , then  $x \leftarrow 2x$ , almost doubling in signal strength. In contrast, if  $x$  and  $f(x)$  are anti-correlated:

$$x + f(x) \approx 0$$

resulting in weaker signal strengths to propagate through the network [31].

After the residual blocks, we reshape the tensor to  $x \in \mathbb{R}^{B \times 2 \times C \times D \times T}$ , which is a four-dimensional tensor. Then, we leverage average pooling across the temporal dimension to form output shape  $x \in \mathbb{R}^{B \times 2 \times C \times D}$ . Thus, each channel has a  $D$ -dimensional feature vector that is a temporal embedding which contains rich representations of EEG signals. Finally, a layer norm is applied per channel to improve stability.

Overall, this module transforms each channel's sequence into a set of latent features [32]. In EEG analysis, 1-D convolutions along the time dimension automatically learn filter banks: they can model band-pass filters and temporal patterns directly from data [33]. The convolution operation can also be interpreted as a learned filter in the frequency domain [32] that allows the network to emphasize patterns like rhythmic bursts or slow drifts. In particular, depthwise per-channel convolutions ensure that each electrode is processed independently and focuses on its own temporal structure. The depthwise convolution layer would pick up on rapid oscillations, while deeper layers integrate these into broader trends [33]. By learning these features end-to-end, the network can discover the relevant frequency and waveform patterns that correlate with fatigue without explicitly computing a Fourier transform [34].

### C. Multilayer Perceptron

In this module, the pooled features of size  $x \in \mathbb{R}^{B \times 2 \times C \times H}$  are flattened to form a tensor of size  $x \in \mathbb{R}^{B \times 2 \times C \cdot H}$ . The two-dimensional tensor is fed into a multilayer perceptron that consists of three sequential blocks, each containing a linear, BatchNorm, LeakyReLU, and Dropout operation to produce three logits that correspond to the three classes. The detailed implementation can be visualized in Fig. 4. We then employ *Softmax* to convert logits to probabilities. The *Softmax* operation is denoted as:

$$\text{Softmax}(x_i) = \frac{\exp(x_i)}{\sum_j \exp(x_j)}$$

where  $i$  denotes the index of the specific class in the output logits for which the output probability is being computed. The

index  $j$  in the summation runs over all elements in the logit vector, ensuring the denominator represents the sum of the exponential of every input element.

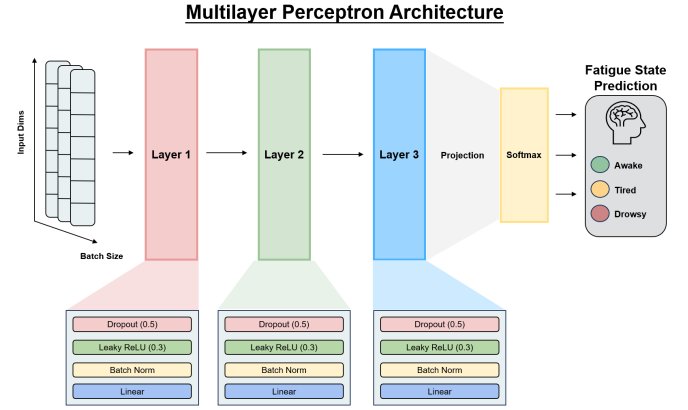


Fig. 4. Structure of Multilayer Perceptron. The multilayer perceptron produces fatigue prediction heads that correspond to the three classes. The input is projected to a dimension of hidden dims. Batch norm is used to prevent internal covariate shift. A leakyReLU activation is used to increase the non-linear representation power of the model. A dropout is used to prevent overfitting to the majority class.

## IV. EXPERIMENTAL DESIGN

### A. Datasets

Two publicly available EEG datasets for vigilance estimation are used in this study: the SEED-VIG dataset and the Sustained-Attention Driving Task (SADT) dataset.

1) *SEED-VIG*: The SEED-VIG dataset [35] is a widely used benchmark for EEG-based driver fatigue detection. Data were collected in a virtual driving environment from 23 subjects (11 male, 12 female, average age 23.3 years). Each subject completed a driving trial lasting approximately 120 minutes, during which EEG signals were recorded from 17 electrode channels at a sampling rate of 200 Hz, following the international 10–20 system.

Fatigue levels were labeled using PERCLOS (percentage of eyelid closure) [36], measured with eye-tracking glasses. Specifically, PERCLOS values from  $p \in (0, 0.35]$  are marked awake,  $p \in (0.35, 0.7]$  are marked tired, and  $p \in (0.7, 1]$  are marked drowsy, where  $p$  denotes the PERCLOS [36] value for that interval. For this study, each trial was divided into 885 samples, each containing 8 seconds of EEG data.

2) *Sustained Attention Driving Task (SADT)*: The SADT dataset [37] was released in 2019 and captures driver behavior and brain activity in a near-realistic simulated driving environment. 27 subjects performed a continuous driving task for up to 90 minutes, during which the vehicle was maintained in the center of the lane. Periodically, lane-deviation events were introduced, requiring drivers to respond quickly to correct the vehicle's position.

Driver fatigue was assessed based on reaction time—the interval between the lane deviation and the driver's corrective response. This metric was used to label each trial as drowsy or alert. We used both versions of the dataset [37], one

which includes 2,952 samples from 11 subjects [38] and one which includes 2022 samples from 11 subjects [39]. Each sample consists of 3 seconds of EEG data (recorded prior to a deviation event) from 30 channels, sampled at 128 Hz.

### B. Baselines

For a comprehensive analysis of our model's superior performance and reproducibility, we compared our model's performance with five benchmark models, spanning from time-series classification models that aim to represent sequential data, deep learning CNN models that capture deep representations of EEG data, and EEG-based models that are tuned specifically for EEG data.

1) *Time Series Classification Models*: FCN Wang [40] is a robust benchmark architecture that is constructed from three sequential convolution blocks, utilizing kernel sizes of 8, 5, and 3, respectively. Moreover, InceptionTime [41] utilizes six stacked inception modules that were inspired by the Inception V4 architecture. Each module integrates parallel convolutional pathways with four distinct kernel sizes. Furthermore, Resnet 1D Wang [40] utilizes an enhanced variant of FCN Wang that incorporates residual connections. In this adaptation, each original convolutional block is expanded to three layers, employing significantly larger kernel sizes of 64, 128, and 256.

2) *Deep Learning CNN and Transformer-Based Models*: Building upon the ResNet architecture [40], the XResnet101 model [42] introduces a modification to its residual blocks. To preserve information during dimensionality reduction, a  $2 \times 2$  average pooling operation with a stride of 2 is incorporated into the downsampling pathway. Vision Transformer (ViT) models an image as a sequence of patches and applies the Transformer self-attention mechanism to capture global visual relationships for image understanding [43].

3) *EEG-Based Models*: EEGNet [44] employs depthwise and separable convolutions to construct a compact and versatile network architecture, which is widely recognized as the state-of-the-art model for diverse EEG classification tasks.

### C. Implementation Details and Evaluation Metrics

The framework used for all experimental work was PyTorch 2.9.0. We used a single A100 GPU from Google Colab and conducted cross-validation experiments to ensure the reproducibility of our results. We used the AdamW optimizer with a  $1e-4$  learning rate and 200 epochs. The batch size was set to 32, and the number of folds for cross-validation was set to 5. For the five folds, we used 60% for training, 20% for validation, and 20% for testing. The split methods can be visualized in Fig 9. For reproducibility concerns, we initialized a random seed of 2026 to ensure identical distributions for each experiment. Our metrics include accuracy, precision, recall, and F1 Score of our samples.

Accuracy measures the overall correctness of predictions across all classes. Precision quantifies how many of the items labeled as positive are actually positive. Recall indicates how many of the truly positive items are correctly identified. F1 Score represents the harmonic mean of precision and recall.

## V. EXPERIMENTAL RESULTS

This section details the evaluation of our proposed model, DeltaGateNet. Performance was assessed through five-fold intra-subject and inter-subject experiments, comparing it against baseline methods from three categories: time series classification models, deep learning CNN/Transformer-based models, and established EEG-specific models. Ablation studies were also conducted to quantify the contribution of each model component.

### A. Comparison Among Previous Models

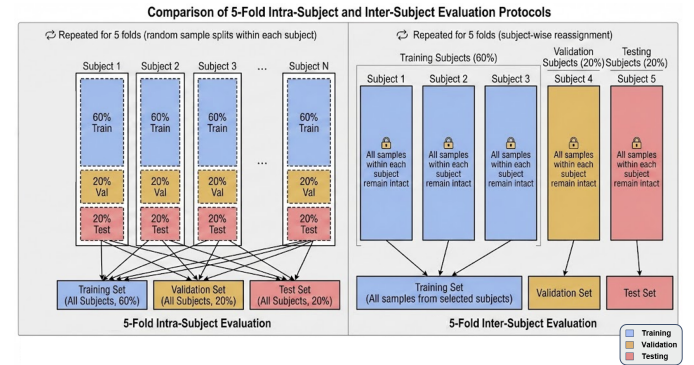


Fig. 5. The figure describes our experimental splits. We conducted thorough experimentation and evaluation by conducting cross-validation with 5 folds to verify the authenticity of our results.

1) *Intra-Subject Experiments*: Table I presents the intra-subject classification performance, evaluated through 5-fold cross-validation, across the SEED-VIG and two SADT datasets for all compared models. The proposed DeltaGateNet consistently achieves the highest performance across all four evaluation metrics on every dataset.

On the SEED-VIG dataset, DeltaGateNet attains an Accuracy of  $81.89 \pm 0.66\%$ , surpassing the next best method (Resnet\_Wang,  $77.64 \pm 0.68\%$ ) by nearly 4 percentage points. It also shows superior gains in Precision (84.37% vs. 78.92%), Recall (81.32% vs. 78.44%), and F1-score (82.55% vs. 78.61%). Moreover, DeltaGateNet achieves dominating performance over models designed to capture EEG signals. DeltaGateNet achieves an eight percent gain over EEGNet on accuracy.

On the SADT 2022 dataset and the SADT 2952 dataset, DeltaGateNet once again surpasses all SOTA models. Surprisingly, time series classification models outperform both EEG-based models and transformer-based models on multiple datasets.

Among baseline models, time series classification methods generally perform well, with InceptionTime and Resnet\_Wang being strong competitors. However, DeltaGateNet maintains a clear and consistent advantage across nearly all metrics, validating its effectiveness in intra-subject fatigue recognition. In comparison, transformer and deep-learning convolution-based models underperform time series models. This suggests that EEG data to measure driving fatigue is not directly correlated with the size or depth of the model.

TABLE I  
INTRA-SUBJECT EVALUATION RESULTS (5-FOLD CROSS-VALIDATION)

Model	SEED-VIG				SADT 2022				SADT 2952			
	Acc	Pre	Rec	F1	Acc	Pre	Rec	F1	Acc	Pre	Rec	F1
EEGNet	73.10 $\pm$ 1.94	75.44 $\pm$ 1.23	73.94 $\pm$ 1.46	73.97 $\pm$ 1.88	76.78 $\pm$ 7.41	81.34 $\pm$ 4.24	76.99 $\pm$ 6.84	75.69 $\pm$ 8.46	88.35 $\pm$ 2.78	89.01 $\pm$ 2.57	87.01 $\pm$ 3.21	87.68 $\pm$ 3.07
FCN_Wang	68.03 $\pm$ 1.19	70.07 $\pm$ 1.62	68.38 $\pm$ 0.75	68.50 $\pm$ 0.97	96.33 $\pm$ 1.65	96.32 $\pm$ 1.63	96.37 $\pm$ 1.61	96.32 $\pm$ 1.64	96.66 $\pm$ 2.06	96.39 $\pm$ 2.20	96.52 $\pm$ 2.29	96.45 $\pm$ 2.24
InceptionTime	77.41 $\pm$ 0.63	79.13 $\pm$ 0.61	77.85 $\pm$ 1.07	78.30 $\pm$ 0.79	94.35 $\pm$ 4.98	94.32 $\pm$ 4.95	94.39 $\pm$ 4.98	94.34 $\pm$ 4.97	95.37 $\pm$ 3.13	95.30 $\pm$ 3.32	95.17 $\pm$ 3.06	95.22 $\pm$ 3.18
Resnet_Wang	77.64 $\pm$ 0.68	78.92 $\pm$ 0.79	78.44 $\pm$ 0.82	78.61 $\pm$ 0.62	93.32 $\pm$ 5.28	92.70 $\pm$ 4.74	93.39 $\pm$ 5.08	92.30 $\pm$ 5.31	94.07 $\pm$ 3.32	94.50 $\pm$ 3.14	92.28 $\pm$ 4.01	93.74 $\pm$ 3.72
XResnet	63.71 $\pm$ 2.42	67.33 $\pm$ 2.01	63.20 $\pm$ 3.14	63.54 $\pm$ 2.66	85.42 $\pm$ 8.05	86.20 $\pm$ 7.57	85.31 $\pm$ 8.12	85.24 $\pm$ 8.22	88.84 $\pm$ 7.24	88.60 $\pm$ 7.43	88.25 $\pm$ 7.61	88.37 $\pm$ 7.50
ViT	71.59 $\pm$ 0.50	73.85 $\pm$ 1.13	71.9 $\pm$ 1.11	72.41 $\pm$ 5.8	86.53 $\pm$ 4.92	86.85 $\pm$ 4.96	86.57 $\pm$ 4.89	86.50 $\pm$ 4.92	88.42 $\pm$ 5.30	88.57 $\pm$ 5.45	87.65 $\pm$ 5.41	87.95 $\pm$ 5.38
<b>DeltaGateNet</b>	<b>81.89 <math>\pm</math> 0.66</b>	<b>84.37 <math>\pm</math> 0.52</b>	<b>81.32 <math>\pm</math> 0.64</b>	<b>82.55 <math>\pm</math> 0.58</b>	<b>96.81 <math>\pm</math> 2.58</b>	<b>96.98 <math>\pm</math> 2.34</b>	<b>96.80 <math>\pm</math> 2.60</b>	<b>96.81 <math>\pm</math> 2.59</b>	<b>96.84 <math>\pm</math> 1.43</b>	<b>96.73 <math>\pm</math> 1.41</b>	<b>96.81 <math>\pm</math> 1.53</b>	<b>96.77 <math>\pm</math> 1.47</b>

2) *Inter-Subject Experiments*: Table II presents the more challenging inter-subject classification results, evaluated through 5-fold cross-subject validation, across the SEED-VIG and SADT datasets. In this rigorous cross-subject paradigm, our proposed DeltaGateNet demonstrates superior generalization by consistently achieving the highest accuracy on all three datasets.

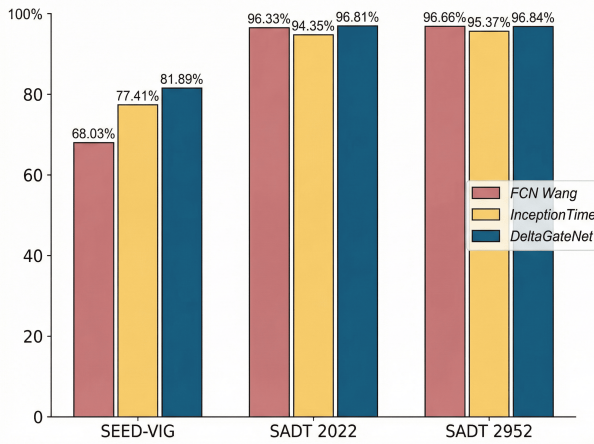


Fig. 6. The diagram illustrates that our model consistently outperforms both InceptionTime and FCN Wang across all three datasets in the intrasubject setting, with our model performing at 81%, 96%, and 96% accuracy respectively across the three datasets.

On SEED-VIG, DeltaGateNet achieves 55.55% accuracy, outperforming the strongest baseline (FCN\_Wang, 48.91%) by approximately 6.64 percentage points, portraying huge gains in performance comparatively.

On SADT 2022, DeltaGateNet attains  $83.21 \pm \%$  accuracy, surpassing InceptionTime (80.12%) by over 3 percentage points with lower variance. Following the InceptionTime model is the ViT model. DeltaGateNet surpasses ViT by 8 percentage points in accuracy, suggesting higher generalization abilities over time series classification models and transformer-based CNN models. On SADT 2952, DeltaGateNet achieves  $84.49 \pm 7.3\%$  Accuracy, exceeding FCN\_Wang ( $82.99 \pm 11.61\%$ ) while showing greater stability by having a smaller variance.

As observed, the margin between first and second place is consistently wider on the SEED-VIG dataset than on SADT. This stems from a fundamental difference in task difficulty: SADT is a binary classification problem, while SEED-VIG is an unfiltered three-class classification. This even more challenging paradigm serves to better demonstrate the advanced learning capabilities of DeltaGateNet.

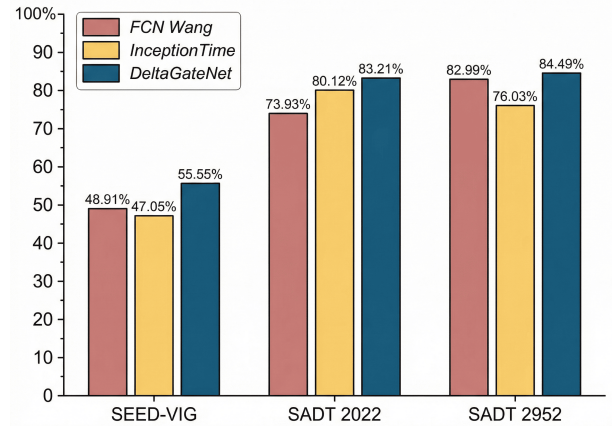


Fig. 7. The diagram illustrates that our model consistently outperforms both InceptionTime and FCN Wang across all three datasets in the intersubject setting, with our model performing at 55%, 83%, and 84% accuracy respectively across the three datasets.

These results confirm that DeltaGateNet not only excels in intra-subject evaluation but also generalizes robustly to unseen subjects, outperforming both specialized EEG models and general time-series classifiers. These intersubject settings are more closely related to real-life detection scenarios. As DeltaGateNet outperforms SOTA models from various fields on multiple datasets, this suggests that DeltaGateNet is deployment-ready to solve real-world problems.

## B. Ablation Studies

1) *Influence of Each Individual Module*: In this section, we conduct a thorough investigation of the learning capabilities of our modules. We conducted rigorous experimentation and analysis of our model. Our results can be summarized in Tables III, IV, V. Furthermore, we evaluate our model on a more challenging inter-subject classification experiment to test our model's generalization across different subjects. As shown in the tables, inter-subject performance is consistently lower than intra-subject performance across all models and datasets, reflecting the difficulty of cross-subject generalization. Despite this, our final model achieves the best performance in all inter-subject settings, demonstrating strong generalization capability.

On Table III, in the intrasubject setting, using only an MLP yields poor performance 43.72%. Adding the Bidirectional Delta module improves the accuracy to 54.03%. The Gated Temporal Convolution + MLP achieves 71.01%, while the full

TABLE II  
INTER-SUBJECT EVALUATION RESULTS (5-FOLD CROSS-SUBJECT VALIDATION)

Model	SEED-VIG					SADT 2022					SADT 2952				
	Acc	Pre	Rec	F1		Acc	Pre	Rec	F1		Acc	Pre	Rec	F1	
EEGNet	44.64 $\pm$ 5.99	46.56 $\pm$ 8.93	43.21 $\pm$ 4.96	39.52 $\pm$ 4.73	68.99 $\pm$ 4.84	74.77 $\pm$ 6.49	68.99 $\pm$ 4.84	67.13 $\pm$ 5.10	77.01 $\pm$ 11.27	79.96 $\pm$ 11.07	76.00 $\pm$ 10.34	75.22 $\pm$ 12.49			
FCN_Wang	48.91 $\pm$ 8.05	50.10 $\pm$ 10.98	48.66 $\pm$ 9.10	46.16 $\pm$ 8.63	73.93 $\pm$ 10.29	75.33 $\pm$ 10.04	73.93 $\pm$ 10.29	73.48 $\pm$ 10.52	82.99 $\pm$ 11.61	82.46 $\pm$ 9.80	83.21 $\pm$ 12.18	81.14 $\pm$ 12.70			
InceptionTime	47.05 $\pm$ 5.38	48.27 $\pm$ 5.26	45.98 $\pm$ 8.42	43.96 $\pm$ 8.73	80.12 $\pm$ 9.11	81.37 $\pm$ 8.28	80.12 $\pm$ 9.11	79.70 $\pm$ 9.71	76.03 $\pm$ 4.12	77.32 $\pm$ 2.30	75.90 $\pm$ 3.46	74.28 $\pm$ 3.55			
Resnet_Wang	45.61 $\pm$ 5.66	42.53 $\pm$ 9.46	44.66 $\pm$ 6.32	41.35 $\pm$ 8.49	72.67 $\pm$ 7.74	74.90 $\pm$ 6.82	72.67 $\pm$ 7.74	71.72 $\pm$ 8.61	72.47 $\pm$ 12.81	74.04 $\pm$ 12.42	71.65 $\pm$ 12.10	71.00 $\pm$ 13.66			
XResnet	45.76 $\pm$ 4.28	48.32 $\pm$ 5.42	44.07 $\pm$ 4.78	42.09 $\pm$ 7.00	64.07 $\pm$ 9.99	72.52 $\pm$ 7.67	64.07 $\pm$ 9.99	58.91 $\pm$ 13.75	66.11 $\pm$ 6.25	68.18 $\pm$ 7.37	61.33 $\pm$ 6.34	58.74 $\pm$ 8.86			
ViT	46.06 $\pm$ 4.62	47.75 $\pm$ 8.24	43.00 $\pm$ 4.90	40.40 $\pm$ 4.27	75.54 $\pm$ 6.38	77.03 $\pm$ 6.25	75.54 $\pm$ 6.38	75.13 $\pm$ 6.65	78.58 $\pm$ 4.60	77.46 $\pm$ 4.64	79.37 $\pm$ 6.28	77.37 $\pm$ 5.04			
<b>DeltaGateNet</b>	<b>55.55 <math>\pm</math> 3.96</b>	<b>54.20 <math>\pm</math> 12.81</b>	<b>48.32 <math>\pm</math> 7.60</b>	<b>47.32 <math>\pm</math> 8.21</b>	<b>83.21 <math>\pm</math> 6.25</b>	<b>84.18 <math>\pm</math> 5.50</b>	<b>83.21 <math>\pm</math> 6.25</b>	<b>83.03 <math>\pm</math> 6.41</b>	<b>84.49 <math>\pm</math> 7.36</b>	<b>85.66 <math>\pm</math> 6.83</b>	<b>83.90 <math>\pm</math> 5.85</b>	<b>83.92 <math>\pm</math> 6.93</b>			

TABLE III  
ABLATION RESULTS ON SEED-VIG (5-FOLD CV)

Intrasubject Evaluation				
Model	Acc	Prec	Rec	F1
MLP	43.72 $\pm$ 0.74	30.87 $\pm$ 2.20	33.35 $\pm$ 0.03	20.46 $\pm$ 0.26
BidirectionalDelta + MLP	54.03 $\pm$ 1.69	64.69 $\pm$ 2.99	45.59 $\pm$ 1.37	43.13 $\pm$ 1.01
GatedTemporalConv + MLP	71.01 $\pm$ 1.12	71.87 $\pm$ 0.96	71.81 $\pm$ 1.26	71.67 $\pm$ 0.96
<b>DeltaGateNet</b>	<b>81.89 <math>\pm</math> 0.66</b>	<b>84.37 <math>\pm</math> 0.52</b>	<b>81.32 <math>\pm</math> 0.64</b>	<b>82.55 <math>\pm</math> 0.58</b>
Intersubject Evaluation				
MLP	43.86 $\pm$ 7.98	24.96 $\pm$ 8.41	33.37 $\pm$ 0.87	22.09 $\pm$ 3.47
Bidirectional Delta + MLP	45.83 $\pm$ 1.77	34.38 $\pm$ 4.08	37.32 $\pm$ 1.39	31.62 $\pm$ 4.46
GatedTemporalConv + MLP	43.37 $\pm$ 4.13	43.54 $\pm$ 5.69	40.98 $\pm$ 3.15	47.32 $\pm$ 8.21
<b>DeltaGateNet</b>	<b>55.55 <math>\pm</math> 3.96</b>	<b>54.20 <math>\pm</math> 12.81</b>	<b>48.32 <math>\pm</math> 7.60</b>	<b>47.32 <math>\pm</math> 8.21</b>

TABLE IV  
ABLATION RESULTS ON SADT 2022 (5-FOLD CV)

Intrasubject Evaluation				
Model	Acc	Prec	Rec	F1
MLP	72.53 $\pm$ 11.83	72.53 $\pm$ 11.98	72.52 $\pm$ 11.97	72.44 $\pm$ 11.97
BidirectionalDelta + MLP	87.71 $\pm$ 13.04	87.72 $\pm$ 13.07	87.66 $\pm$ 13.15	87.64 $\pm$ 13.17
GatedTemporalConv + MLP	92.17 $\pm$ 2.94	92.28 $\pm$ 3.01	92.17 $\pm$ 2.99	92.15 $\pm$ 2.95
<b>DeltaGateNet</b>	<b>96.81 <math>\pm</math> 2.58</b>	<b>96.98 <math>\pm</math> 2.34</b>	<b>96.80 <math>\pm</math> 2.60</b>	<b>96.81 <math>\pm</math> 2.59</b>
Intersubject Evaluation				
MLP	69.73 $\pm$ 10.06	71.61 $\pm$ 7.16	69.73 $\pm$ 10.06	66.62 $\pm$ 15.90
Bidirectional Delta + MLP	75.03 $\pm$ 13.83	71.63 $\pm$ 19.22	70.74 $\pm$ 18.89	70.35 $\pm$ 19.10
GatedTemporalConv + MLP	79.51 $\pm$ 1.76	80.53 $\pm$ 1.60	79.51 $\pm$ 1.76	79.34 $\pm$ 1.85
<b>DeltaGateNet</b>	<b>83.21 <math>\pm</math> 6.25</b>	<b>84.18 <math>\pm</math> 5.50</b>	<b>83.21 <math>\pm</math> 6.25</b>	<b>83.03 <math>\pm</math> 6.41</b>

DeltaGateNet reaches 81.89%, demonstrating the synergistic effect of both modules. This proves that our modules are capable of extracting features from different latent spaces. The Bidirectional Delta Module is able to improve the model's accuracy by 11% demonstrating the robust capabilities of this module. Not only does it improve the performance of simple models such as MLP, but it also consists of no learnable parameters, leading to a more efficient design. On intersubject settings, our model improves Accuracy by 9.72% over the next best baseline (Bidirectional Delta + MLP), demonstrating similar learning capabilities on intrasubject settings.

On SADT 2022 IV, in the intrasubject setting, the full model achieves 96.81% Accuracy, compared to 92.17% for Gated Temporal Conv + MLP and 87.71% for Bidirectional Delta + MLP. This demonstrates its superior performance on bi-classification datasets, outperforming many SOTA models despite its simple design. In intersubject settings, the full model achieves 83.21% Accuracy, compared to 79.51% for Gated Temporal Conv + MLP and 75.03% for Bidirectional Delta + MLP, showcasing its cross-domain capabilities on bi-classification datasets and its readiness for real-world driving scenarios.

On SADT 2952 V, the full model again shows the best performance, confirming that both Bidirectional temporal mod-

TABLE V  
ABLATION RESULTS ON SADT 2952 (5-FOLD CV)

Intrasubject Evaluation				
Model	Acc	Prec	Rec	F1
MLP	74.30 $\pm$ 8.73	74.71 $\pm$ 10.33	71.36 $\pm$ 9.14	71.68 $\pm$ 10.09
BidirectionalDelta + MLP	87.07 $\pm$ 10.12	86.17 $\pm$ 11.08	86.18 $\pm$ 11.26	86.14 $\pm$ 11.17
GatedTemporalConv + MLP	93.30 $\pm$ 3.35	93.43 $\pm$ 2.95	92.86 $\pm$ 3.80	92.99 $\pm$ 3.52
<b>DeltaGateNet</b>	<b>96.84 <math>\pm</math> 1.43</b>	<b>96.73 <math>\pm</math> 1.41</b>	<b>96.81 <math>\pm</math> 1.53</b>	<b>96.77 <math>\pm</math> 1.47</b>
Intersubject Evaluation				
MLP	70.28 $\pm$ 12.88	69.98 $\pm$ 14.39	65.25 $\pm$ 10.71	65.87 $\pm$ 12.16
Bidirectional Delta + MLP	81.05 $\pm$ 14.05	80.10 $\pm$ 14.06	78.16 $\pm$ 13.20	78.78 $\pm$ 13.45
GatedTemporalConv + MLP	77.54 $\pm$ 8.46	78.93 $\pm$ 3.65	78.94 $\pm$ 5.89	76.55 $\pm$ 8.13
<b>DeltaGateNet</b>	<b>84.49 <math>\pm</math> 7.36</b>	<b>85.66 <math>\pm</math> 6.83</b>	<b>83.90 <math>\pm</math> 5.85</b>	<b>83.92 <math>\pm</math> 6.93</b>

eling and channel-wise encoding are essential for capturing fatigue-related dynamics. DeltaGateNet attains 84.49% Accuracy, outperforming Gated Temporal Conv + MLP 77.54% and Bidirectional Delta + MLP 81.05% on intersubject settings. Its performance is even more pronounced in the intrasubject setting, where its accuracy reaches an astonishing 96.84%.

These ablation results consistently show that both the Bidirectional Delta and Gated Temporal Convolution modules contribute significantly to model performance, with the full integration yielding the highest accuracy and robustness in both intra and inter-subject evaluations. Moreover, their combination outperforms SOTA models, highlighting their capability of learning richer representations from different latent spaces.

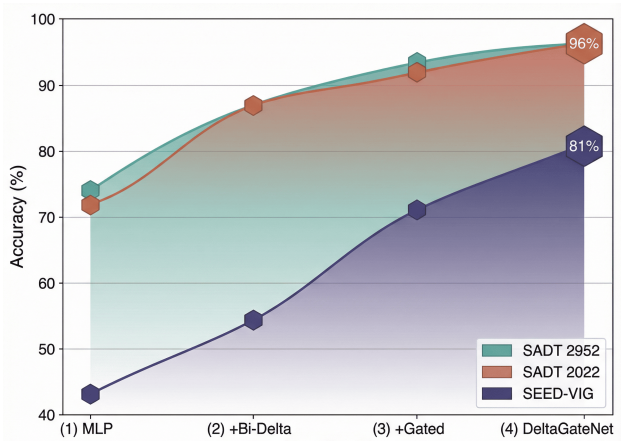


Fig. 8. The diagram illustrates the progressive performance gain achieved by incrementally adding our proposed modules on the intrasubject experiments, demonstrating their effectiveness. Our model achieves 96% accuracy on SADT datasets and 81% on the SEED-VIG dataset.

2) *Ablation Studies for Parameter Analysis:* In addition to a comprehensive comparison of our model with SOTA models, we have also conducted investigations to inspect

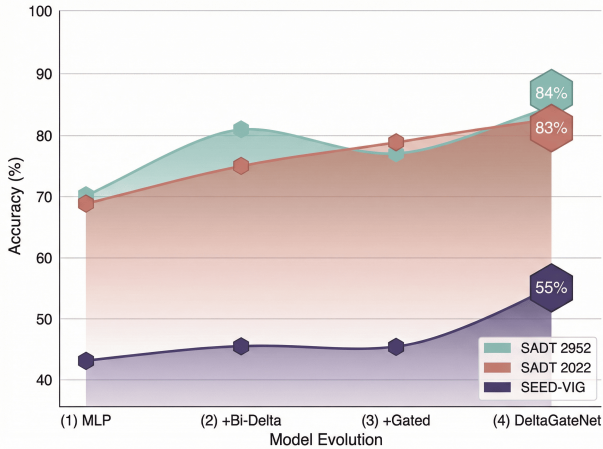


Fig. 9. The diagram illustrates the progressive performance gain achieved by incrementally adding our proposed modules on the intersubject experiments, demonstrating their effectiveness. Our model achieves 83% accuracy on SADT datasets and 55% on the SEED-VIG dataset.

TABLE VI  
KERNEL SIZE TUNING ON SEED-VIG (5-FOLD CV)

Intrasubject Evaluation				
Kernel Size	Acc	Prec	Rec	F1
K = 1	71.08 $\pm$ 3.86	74.39 $\pm$ 2.37	68.30 $\pm$ 5.48	69.58 $\pm$ 4.83
K = 3	73.04 $\pm$ 3.81	77.27 $\pm$ 3.57	70.43 $\pm$ 5.01	72.12 $\pm$ 4.77
K = 5	74.14 $\pm$ 3.74	78.26 $\pm$ 3.29	71.87 $\pm$ 5.01	73.52 $\pm$ 4.68
<b>K = 7</b>	<b>81.89<math>\pm</math>0.66</b>	<b>84.37<math>\pm</math>0.52</b>	<b>81.32<math>\pm</math>0.64</b>	<b>82.55<math>\pm</math>0.58</b>
Intersubject Evaluation				
Kernel Size	Acc	Prec	Rec	F1
K = 1	48.73 $\pm$ 4.03	49.30 $\pm$ 9.92	42.36 $\pm$ 5.44	37.72 $\pm$ 5.58
K = 3	48.12 $\pm$ 4.27	49.08 $\pm$ 11.38	41.00 $\pm$ 4.58	37.10 $\pm$ 5.30
K = 5	43.37 $\pm$ 4.13	43.54 $\pm$ 5.69	40.98 $\pm$ 3.15	47.32 $\pm$ 8.21
<b>K = 7</b>	<b>55.55<math>\pm</math>3.96</b>	<b>54.20<math>\pm</math>12.81</b>	<b>48.32<math>\pm</math>7.60</b>	<b>47.32<math>\pm</math>8.21</b>

the functionalities of our model. We conducted experiments testing the kernel size of the gated temporal convolution module and the step size of the Bidirectional delta module, gaining insight into why the model works. These experiments provide critical insight into the model's operational mechanics and the synergistic relationship between its components.

We experiment with kernel sizes  $K \in \{1, 3, 5, 7\}$ , where  $K$  denotes the one dimensional kernel size. We also experiment with step sizes  $S \in \{1, 2, 3\}$  where  $S$  denotes the step size of the Bidirectional module.

Turning to tables VI and VII for the SEED-VIG dataset, we can see that parameters increased 10% on intrasubject evaluation when kernel size started from  $K = 1$  and ended at  $K = 7$ . Similar effects are shown on the intersubject evaluation paradigm as well. As for the step size, we are shown that the accuracy decreases with larger step sizes. We believe that this is because the approximation for the differential becomes less robust as the step size increases.

Tables VIII and IX show our parameter analysis for the SADT 2022 dataset. We can see that as the parameters approach our optimal parameters, not only does the accuracy increase gradually, but the variance also decreases concurrently, suggesting higher stability. The parameter analysis for the SADT 2952 dataset X XI concurs with the fact that our parameters are optimal.

TABLE VII  
STEP SIZE TUNING ON SEED-VIG (5-FOLD CV)

Intrasubject Evaluation				
Step Size	Acc	Prec	Rec	F1
<b>S = 1</b>	<b>81.89<math>\pm</math>0.66</b>	<b>84.37<math>\pm</math>0.52</b>	<b>81.32<math>\pm</math>0.64</b>	<b>82.55<math>\pm</math>0.58</b>
S = 2	78.11 $\pm$ 2.89	80.82 $\pm$ 1.81	77.47 $\pm$ 3.57	78.62 $\pm$ 3.14
S = 3	78.10 $\pm$ 2.41	80.55 $\pm$ 1.69	77.67 $\pm$ 2.98	78.69 $\pm$ 2.61
Intersubject Evaluation				
Step Size	Acc	Prec	Rec	F1
<b>S = 1</b>	<b>55.55<math>\pm</math>3.96</b>	<b>54.20<math>\pm</math>12.81</b>	<b>48.32<math>\pm</math>7.60</b>	<b>47.32<math>\pm</math>8.21</b>
S = 2	49.16 $\pm$ 7.14	53.21 $\pm$ 10.90	44.43 $\pm$ 8.11	41.30 $\pm$ 6.49
S = 3	47.51 $\pm$ 8.76	50.25 $\pm$ 11.32	43.16 $\pm$ 7.15	39.33 $\pm$ 7.19

TABLE VIII  
KERNEL SIZE TUNING ON SADT 2022 (5-FOLD CV)

Intrasubject Evaluation				
Kernel Size	Acc	Prec	Rec	F1
K = 1	94.92 $\pm$ 2.07	94.97 $\pm$ 2.02	94.95 $\pm$ 2.09	94.90 $\pm$ 2.07
K = 3	96.56 $\pm$ 2.08	96.97 $\pm$ 2.03	96.95 $\pm$ 2.14	96.81 $\pm$ 2.59
K = 5	96.16 $\pm$ 2.24	96.18 $\pm$ 2.34	96.16 $\pm$ 2.23	96.15 $\pm$ 2.24
<b>K = 7</b>	<b>96.81<math>\pm</math>2.58</b>	<b>96.98<math>\pm</math>2.34</b>	<b>96.80<math>\pm</math>2.60</b>	<b>96.81<math>\pm</math>2.59</b>
Intersubject Evaluation				
Kernel Size	Acc	Prec	Rec	F1
K = 1	65.72 $\pm$ 17.05	67.64 $\pm$ 20.15	63.34 $\pm$ 21.36	62.87 $\pm$ 20.17
K = 3	74.45 $\pm$ 8.41	79.30 $\pm$ 5.73	74.45 $\pm$ 8.41	72.84 $\pm$ 9.81
K = 5	82.25 $\pm$ 11.86	88.26 $\pm$ 6.88	85.25 $\pm$ 11.86	84.10 $\pm$ 14.05
<b>K = 7</b>	<b>83.21<math>\pm</math>6.25</b>	<b>84.18<math>\pm</math>5.50</b>	<b>83.21<math>\pm</math>6.25</b>	<b>83.03<math>\pm</math>6.41</b>

The results confirm that the configuration  $S = 1$  and  $K = 7$  yield superior performance across both intrasubject and intersubject evaluation paradigms. The temporal convolution  $K = 7$  captures broad textual patterns while the fine-grained delta module  $S = 1$  extracts critical short-term Bidirectional changes. Their fused representation provides a robust and comprehensive feature space for vigilance estimation.

## VI. CONCLUSION

In this paper, a bidirectional temporal dynamics modeling framework with gated temporal encoding is proposed for EEG-based driving fatigue recognition. First, we introduce a Bidirectional Delta module to decompose first-order temporal differentials into positive and negative components, explicitly modeling asymmetric neural activation and suppression patterns associated with vigilance degradation. Second, we design a Gated Temporal Convolution module that learns long-term temporal dependencies for each EEG channel using depthwise temporal convolutions and residual learning, preserving spatial specificity while enhancing temporal representation robustness under limited channel configurations. Third, we present a complete framework that effectively integrates Bidirectional temporal dynamics with channel-wise temporal encoding, improving both interpretability and generalization capability for cross-subject (intersubject) scenarios. Extensive experiments conducted under both intrasubject and intersubject evaluation settings on SADT and SEED-VIG datasets demonstrate that our proposed approach consistently outperforms existing methods. In future work, we will consider multimodal physiological signal data as input and construct a more general model for driving fatigue recognition. We will also work on integrating environmental information with physiological data for a more comprehensive evaluation of fatigue states.

TABLE IX  
STEP SIZE TUNING ON SADT 2022 (5-FOLD CV)

Intrasubject Evaluation				
Step Size	Acc	Prec	Rec	F1
<b>S = 1</b>	<b>96.81±2.58</b>	<b>96.98±2.34</b>	<b>96.80±2.60</b>	<b>96.81±2.59</b>
S = 2	95.60±2.63	95.67±2.53	95.61±2.65	95.60±2.63
S = 3	95.12±2.79	95.13±2.81	95.16±2.80	95.12±2.80
Intersubject Evaluation				
Step Size	Acc	Prec	Rec	F1
<b>S = 1</b>	<b>83.21±6.25</b>	<b>84.18±5.50</b>	<b>83.21±6.25</b>	<b>83.03±6.41</b>
S = 2	75.422±8.95	78.00±7.02	75.42±8.95	74.42±10.05
S = 3	81.28±12.27	82.60±12.04	81.28±12.27	81.03±12.38

TABLE X  
KERNEL SIZE TUNING ON SADT 2952 (5-FOLD CV)

Intrasubject Evaluation				
Kernel Size	Acc	Prec	Rec	F1
K = 1	95.69±1.76	95.66±1.79	95.50±1.70	95.55±1.75
K = 3	95.75±1.85	95.65±1.99	95.62±1.84	95.62±1.91
K = 5	96.70±1.73	96.59±1.87	96.67±1.67	96.61±1.78
<b>K = 7</b>	<b>96.84±1.43</b>	<b>96.73±1.41</b>	<b>96.81±1.53</b>	<b>96.77±1.47</b>
Intersubject Evaluation				
Kernel Size	Acc	Prec	Rec	F1
K = 1	78.74±6.78	79.76±7.22	78.01±7.99	77.25±8.22
K = 3	63.88±21.13	64.88±19.83	65.45±20.71	62.13±22.21
K = 5	77.75±8.82	79.56±6.16	78.51±7.90	76.91±9.02
<b>K = 7</b>	<b>84.49±7.36</b>	<b>85.66±6.83</b>	<b>83.90±5.85</b>	<b>83.92±6.93</b>

## ACKNOWLEDGMENTS

## REFERENCES

- [1] M.E. Shaik, "A systematic review on detection and prediction of driver drowsiness," *Transp. Res. Interdiscip. Perspect.*, vol. 21, Art. no. 100864, 2023.
- [2] M. Sprajcer, et al., "How tired is too tired to drive? A systematic review assessing the use of prior sleep duration to detect driving impairment," *Nat. Sci. Sleep*, vol. 15, no. 2, pp. 175–206, 2023.
- [3] M.S. Al-Quraishi, S.S.A. Ali, A. Muhammad, T.B. Tang, and S. Elferik, "Technologies for detecting and monitoring drivers' states: A systematic review," *Heliyon*, vol. 10, no. 20, 2024.
- [4] O.O. Ajayi, A.M. Kurien, K. Djouani, and L. Dieng, "A multimodal systematic review of drivers' fatigue detection methodologies, datasets, and models," *IEEE Access*, 2025.
- [5] Z. Tian, N.S. Albakry, and Y. Du, "Illumination intelligent adaptation and analysis framework: A comprehensive solution for enhancing nighttime driving fatigue monitoring," *PLoS ONE*, vol. 19, no. 8, Art. no. e0308201, 2024.
- [6] D. Yu, W. Wang, T. Ding, Z. Niu, J. Zhi, X. Xie, Z. Zhang, X. Tang, and D. Yu, "An application study of a DynGraph-TF-Based EEG recognition framework for predicting mental fatigue in train drivers," *Adv. Eng. Inform.*, vol. 68, Art. no. 103675, 2025.
- [7] Y. Cao, T. Chen, K. Han, H. Chung, Z. Huang, and H. Ding, "SET-DGCN: An end-to-end electroencephalography-based fatigue detection method for young drivers," *Accid. Anal. Prev.*, vol. 225, Art. no. 108311, 2026.
- [8] J. Hu, M.M.U. Rahman, and T.-M. Laleg-Kirati, "Adaptive long-range modeling of EEG and ECG with Mamba and dynamic graph learning," *Scientific Reports*, vol. 15, no. 1, Art. no. 38762, 2025.
- [9] J. Wang, S. Zhao, Z. Luo, Y. Zhou, S. Li, and G. Pan, "Eegmamba: An eeg foundation model with mamba," *Neural Networks*, Art. no. 107816, 2025.
- [10] B. Gao, Y. Yan, C. Huangfu, J. Cai, and H. Wang, "IDSRN: Interpretable dynamic system recurrent network for driver fatigue assessment," *Applied Sciences*, vol. 15, no. 21, Art. no. 11384, 2025.
- [11] O.E. Krigolson, H. Howse, M.R. Hammerstrom, A. Walzak, B. Wright, and K.G. Hecker, "Using EEG to assess cognitive fatigue in real time: A medical simulation study," *Medical Science Educator*, pp. 1–9, 2025.
- [12] I. Babu Henry Samuel, C. Wang, S.E. Burke, B. Kluger, and M. Ding, "Compensatory neural responses to cognitive fatigue in young and older adults," *Frontiers in Neural Circuits*, vol. 13, Art. no. 12, 2019.
- [13] T. Liu, Y. Wu, A. Ye, L. Cao, and Y. Cao, "Two-stage sparse multi-objective evolutionary algorithm for channel selection optimization in BCIs," *Frontiers in Human Neuroscience*, vol. 18, Art. no. 1400077, 2024.
- [14] W.M. Shalash, "A deep learning cnn model for driver fatigue detection using single EEG channel," *J. Theor. Appl. Inf. Technol.*, vol. 99, no. 2, pp. 462–477, 2021.
- [15] A.V. Parekkattil, S.K. Varun, and T.K.R. Bollu, "EEG-based reaction time prediction using covariance augmented 2D convolutional neural network," in \*International Conference on Pattern Recognition\*, pp. 296–310, 2024.
- [16] J. Cui, Z. Lan, Y. Liu, R. Li, F. Li, O. Sourina, and W. Müller-Wittig, "A compact and interpretable convolutional neural network for cross-subject driver drowsiness detection from single-channel EEG," *Methods*, vol. 202, pp. 173–184, 2022.
- [17] Y. Sun, M. Ke, and L. Wang, "A novel inceptionTime framework for multimodal physiological signal-based mental state recognition using wearable device," in \*Proceedings of the 2025 5th International Conference on Bioinformatics and Intelligent Computing\*, pp. 563–570, 2025.
- [18] J. Tang, W. Zhou, W. Zheng, Z. Zeng, J. Li, R. Su, T. Adili, W. Chen, C. Chen, and J. Luo, "Attention-guided multiscale convolutional neural network for driving fatigue detection," *IEEE Sensors J.*, vol. 24, no. 14, pp. 23280–23290, 2024.
- [19] Z. Wang, X. Du, C. Jiang, and J. Sun, "Research on the prediction of driver fatigue degree based on EEG signals," *Sensors*, vol. 25, no. 23, Art. no. 7316, 2025.
- [20] W. Yang, X. Wang, W. Qi, and W. Wang, "LGFormer: integrating local and global representations for EEG decoding," *J. Neural Eng.*, vol. 22, no. 2, Art. no. 026042, 2025.
- [21] E. Modesitt, H. Yin, W. Huang Wang, and B. Lu, "Fusing pretrained ViTs with TCNet for enhanced EEG regression," in \*International Conference on Human-Computer Interaction\*, pp. 47–59, 2024.
- [22] V.J. Lawhern, A.J. Solon, N.R. Waytowich, S.M. Gordon, C.P. Hung, and B.J. Lance, "EEGNet: a compact convolutional neural network for EEG-based brain–computer interfaces," *J. Neural Eng.*, vol. 15, no. 5, Art. no. 056013, 2018.
- [23] S. Hana, R. Hassan, A.R. Faizabadi, A. Gubbi, M.Z. Bellary, and V. Manjula, "Enhanced EEGNet optimization using lightweight deep neural network for detecting human stress levels from raw EEG signals dataset," in \*2025 3rd International Conference on Integrated Circuits and Communication Systems (ICICACS)\*, pp. 1–6, 2025.
- [24] G. Kim and S. Choi, "Sound Event Detection Using Derivative Features in Deep Neural Networks," *Appl. Sci.*, vol. 10, no. 14, p. 4911, Jul. 2020.
- [25] A. J. Anderson, C. Davis, and E. C. Lalor, "Deep-learning models reveal how context and listener attention shape electrophysiological correlates of speech-to-language transformation," *PLOS Comput. Biol.*, vol. 20, no. 11, p. e1012537, Nov. 2024.
- [26] Y. N. Dauphin, A. Fan, M. Auli, and D. Grangier, "Language Modeling with Gated Convolutional Networks," arXiv, preprint arXiv:1612.08083, Dec. 2016.
- [27] A. van den Oord, S. Dieleman, H. Zen, K. Simonyan, O. Vinyals, A. Graves, N. Kalchbrenner, A. Senior, and K. Kavukcuoglu, "WaveNet: A Generative Model for Raw Audio," arXiv, preprint arXiv:1609.03499, Sep. 2016.
- [28] Z. Wu, S. Pan, G. Long, J. Jiang, and C. Zhang, "Graph WaveNet for Deep Spatial-Temporal Graph Modeling," arXiv, preprint arXiv:1906.00121, May 2019
- [29] D. Hendrycks and K. Gimpel, "Gaussian Error Linear Units (GELUs)," arXiv, preprint arXiv:1606.08415, Jun. 2016.

TABLE XI  
STEP SIZE TUNING ON SADT 2952 (5-FOLD CV)

Intrasubject Evaluation				
Step Size	Acc	Prec	Rec	F1
<b>S = 1</b>	<b>96.84±1.43</b>	<b>96.73±1.41</b>	<b>96.81±1.53</b>	<b>96.77±1.47</b>
S = 2	95.93±1.76	95.77±1.83	95.92±1.78	95.84±1.81
S = 3	95.90±0.84	95.89±0.75	95.66±1.05	95.74±0.87
Intersubject Evaluation				
Step Size	Acc	Prec	Rec	F1
<b>S = 1</b>	<b>84.49±7.36</b>	<b>85.66±6.83</b>	<b>83.90±5.85</b>	<b>83.92±6.93</b>
S = 2	81.66±10.16	82.23±10.38	81.62±10.00	81.22±10.11
S = 3	81.70±12.25	83.53±9.42	81.90±10.49	79.69±12.39

- [30] K. He, X. Zhang, S. Ren, and J. Sun, “Deep Residual Learning for Image Recognition,” in Proc. IEEE Conf. Comput. Vis. Pattern Recognit. (CVPR), Jun. 2016.
- [31] S. Balduzzi, M. Frean, L. Leary, J. Lewis, K. W.-D. Ma, and B. McWilliams, “The Shattered Gradients Problem: If ResNets Are the Answer, Then What Is the Question?” in Proc. Int. Conf. Mach. Learn. (ICML), Jul. 2017.
- [32] C. Liu et al., “A compact multi-branch 1D convolutional neural network for EEG-based motor imagery classification,” *Biomed. Signal Process. Control*, vol. 80, pt. 1, p. 104270, Mar. 2023.
- [33] O. B. Guney et al., “GDNet-EEG: An attention-aware deep neural network based on group depth-wise convolution for SSVEP stimulation frequency recognition,” *Front. Neurosci.*, vol. 17, p. 1160040, Apr. 2023.
- [34] D. Gao et al., “EEG driving fatigue detection based on log-Mel spectrogram and convolutional recurrent neural networks,” *Front. Neurosci.*, vol. 17, p. 1136609, Mar. 2023.
- [35] W. Zheng and B. Lu, “A multimodal approach to estimating vigilance using EEG and forehead EOG,” *J. Neural Eng.*, vol. 14, no. 2, Feb. 2017, Art. no. 026017.
- [36] D. Dinges and R. Grace, “PERCLOS: A valid psychophysiological measure of alertness as assessed by psychomotor vigilance,” US Dept. Transp., Federal Highway Admin., Tech. Rep. FHWA-MCRT-98-006, 1998.
- [37] Z. Gao, C. Chuang, J. King, and C. Lin, “Multi-channel EEG recordings during a sustained-attention driving task,” *Sci. Data*, vol. 19, no. 6, pp. 1–10, Apr. 2019.
- [38] Cui, Jian (2021). EEG driver drowsiness dataset (unbalanced). figshare. Dataset. <https://doi.org/10.6084/m9.figshare.16586957.v1>
- [39] Cui, Jian (2021). EEG driver drowsiness dataset. figshare. Dataset. <https://doi.org/10.6084/m9.figshare.14273687.v3>
- [40] Z. Wang, W. Yan, and T. Oates, “Time series classification from scratch with deep neural networks,” in *Proc. Int. Joint Conf. Neural Netw. (IJCNN)*, 2017, pp. 1578–1585.
- [41] H. Ismail Fawaz et al., “InceptionTime: Finding AlexNet for time series classification,” *Data Mining Knowl. Discov.*, vol. 34, no. 6, pp. 1936–1962, 2020.
- [42] T. He, Z. Zhang, H. Zhang, Z. Zhang, J. Xie, and M. Li, “Bag of tricks for image classification with convolutional neural networks,” in *Proc. IEEE/CVF Conf. Comput. Vis. Pattern Recognit. (CVPR)*, Jun. 2019, pp. 558–567.
- [43] A. Dosovitskiy, L. Beyer, A. Kolesnikov, D. Weissenborn, X. Zhai, T. Unterthiner, M. Dehghani, M. Minderer, G. Heigold, S. Gelly, J. Uszkoreit, and N. Houlsby, “An Image Is Worth 16 $\times$ 16 Words: Transformers for Image Recognition at Scale,” in Proc. Int. Conf. Learn. Represent. (ICLR), Apr. 2021.
- [44] V. J. Lawhern et al., “EEGNet: A compact convolutional neural network for EEG-based brain-computer interfaces,” *J. Neural Eng.*, vol. 15, no. 5, Art. no. 056013, 2018.